Learned 2D-TwISTA for 2-D Sparse ISAR Imaging

Quan Huang, Lei Zhang, Shaopeng Wei, *Associate Member, IEEE*, and Jia Duan

***Abstract*— By unfolding traditional optimization algorithms into the form of neural networks, the unfolding network methods have attracted more and more attention in sparse inverse synthetic aperture radar (ISAR) imaging because of their high reconstruction performance and good interpretability. However, existing unfolding network methods mainly focus on 1-D sparse ISAR imaging and cannot be directly applied to 2-D sparse ISAR data. For this reason, a novel learned 2D-two-step iterative shrinkage/thresholding algorithm (L-2D-TwISTA) is proposed for high-efficiency and high-accuracy 2-D sparse ISAR imaging. Specifically, each stage of L-2D-TwISTA corresponds to an iterative solution step of the developed 2D-TwISTA approach. Moreover, a complex-valued (CV) residual network is designed in L-2D-TwISTA to improve training efficiency and solve the nonlinear problem of proximal mapping of the 2D-TwISTA more effectively. The experimental results of real-measured data confirm that the L-2D-TwISTA can realize high-performance 2-D sparse ISAR imaging.**

***Index Terms*— 2-D sparse inverse synthetic aperture radar (ISAR) imaging, 2D-two-step iterative shrinkage thresholding algorithm (2D-TwISTA), learned 2D-TwISTA.**

I. Introduction

INVERSE synthetic aperture radar (ISAR) imaging can effectively obtain 2-D images of noncooperative targets [1], [2], [3], [4], [5], [6]. For conventional ISAR technology, the range resolution of the generated image is proportional to the radar transmitted signal bandwidth, which will increase the burden on the radar hardware system under conditions of high range resolution. The sparse stepped-frequency modulation waveform [5] is an effective approach for solving this problem. However, in this case, the received radar echo is sparse in the range direction. In addition, due to strong interference signals and other reasons [6], [7], [8], sparse aperture (SA) of radar echoes usually appears in the cross-range direction. Based on the above factors, developing methods suitable for 2-D sparse ISAR imaging is necessary.

For addressing the issue of 2-D sparse ISAR imaging, 2-D compressive sampling (CS) is a useful method. The traditional 2-D CS optimization methods for 2-D sparse ISAR imaging mainly include the alternating direction multiplier method (ADMM), iterative shrinkage/thresholding algorithm (ISTA), fast sparse Bayesian learning (SBL), and so on [2], [3], [4], [5], [6], [7]. A 2D-ADMM method is proposed in [2] for high-resolution ISAR imaging, which aims to overcome the shortcomings of high memory use and low computational efficiency of 1-D CS methods. A fast SBL/iterative Wiener filter (IWF)-based approach is proposed in [6] for 2-D joint super-resolution ISAR imaging, which does not utilize any approximation compared with other fast SBL algorithms. The above methods have achieved good 2-D sparse ISAR imaging results. Although fast SBL algorithms are more effective than traditional SBL methods, they may not fulfill the conditions of real-time ISAR imaging systems. The 2D-ADMM method utilizes matrix form to implement the algorithm and usually needs to manually adjust the optimization parameters to achieve better results, which may lead to low operational efficiency.

Compared with traditional CS methods, the unfolding network is an efficient sparse ISAR imaging approach and has attracted growing attention. A self-supervised parallel ISTA-Net is proposed in [9] for SA ISAR imaging. An integrated deep convolution and unfolding network based on the approximate message-passing algorithm is proposed in [10]. Although these methods can acquire satisfactory SA ISAR imaging results, they cannot be directly used for 2-D sparse ISAR imaging. A 2D-ADMM-based unfolding network method is proposed in [11]. However, the nonlinear problem of proximal mapping is implemented using a soft thresholding function module, which may lead to low training efficiency and network performance degradation when the ISAR image amplitude distribution is uneven.

This letter proposes a novel 2-D sparse ISAR imaging method based on the learned 2D-two-step ISTA (L-2D-TwISTA) to handle the above problems. First, a 2D-TwISTA method is developed based on the conventional TwISTA [12]. Then, the 2D-TwISTA is iteratively unfolding into one stage of the L-2D-TwISTA. On this basis, a complex-valued (CV) residual network is designed to solve the nonlinear problem of the proximal mapping of the 2D-TwISTA, which can improve the training efficiency and effectively enhance the ISAR image feature representation capability. The main contributions of this letter are outlined as follows.

1) Based on the traditional TwISTA, a novel 2D-TwISTA approach is developed for 2-D sparse ISAR imaging. The 2D-TwISTA can process different 2-D sparse ISAR sampling [such as 2-D random missing sampling (2D-RMS) and 2-D gap missing sampling (2D-GMS)]

Received 28 November 2024; revised 31 January 2025; accepted 27 February 2025. Date of publication 4 March 2025; date of current version 14 March 2025. This work was supported in part by the National Natural Science Foundation of China under Grant 62301612, Grant 62101603, and Grant 62201623; and in part by the Natural Science Foundation of Shandong Province under Grant ZR2023QF004. *(Corresponding authors: Lei Zhang; Shaopeng Wei.)*

Quan Huang, Lei Zhang, and Jia Duan are with the School of Electronics and Communication Engineering, Sun Yat-sen University, Shenzhen 518107, China (e-mail: huangq267@mail2.sysu.edu.cn; zhanglei57@mail.sysu.edu.cn; bifiduan119@126.com).

Shaopeng Wei is with the College of Oceanography and Space Informatics, China University of Petroleum (East China), Qingdao 266580, China (e-mail: spwei@upc.edu.cn).

Digital Object Identifier 10.1109/LGRS.2025.3547408

1558-0571 © 2025 IEEE. All rights reserved, including rights for text and data mining, and training of artificial intelligence and similar technologies. Personal use is permitted, but republication/redistribution requires IEEE permission.
See https://www.ieee.org/publications/rights/index.html for more information.
Authorized licensed use limited to: SUN YAT-SEN UNIVERSITY. Downloaded on March 15,2025 at 02:07:22 UTC from IEEE Xplore. Restrictions apply.

data without requiring changes to the algorithm model. Moreover, the proposed L-2D-TwISTA method can also use a single trained model to process ISAR data from two different sparse sampling patterns simultaneously. The Fourier transform matrix in 2D-TwISTA and L-2D-TwISTA can be implemented using the fast Fourier transform (FFT), effectively improving computational efficiency.

2) For 2D-TwISTA, choosing appropriate optimization parameters can be difficult sometimes, and it often takes multiple iterations to achieve good ISAR imaging results. Based on 2D-TwISTA, L-2D-TwISTA is proposed for efficient 2-D sparse ISAR imaging, where all parameters are learned from the 2-D sparse ISAR data. The proposed L-2D-TwISTA not only allows for high-accuracy ISAR image recovery but also provides good interpretability.

II. Methodology

A. Traditional TwISTA

First, the traditional TwISTA for CS reconstruction is illustrated. Compared with the classic ISTA, the TwISTA has the advantages of faster convergence and higher CS reconstruction performance, specifically in ill-conditioned problems [12]. The optimization issue of CS reconstruction can be expressed as

$$\hat{\boldsymbol{x}} = \arg\min_{\boldsymbol{x}} \left\{ \frac{1}{2}\|\boldsymbol{\Phi}\boldsymbol{x} - \boldsymbol{y}\|_2^2 + \lambda\Psi(\boldsymbol{x}) \right\} \tag{1}$$

where $\boldsymbol{y}$ is the CS measurements, $\boldsymbol{\Phi}$ represents the CS sampling matrix, $\boldsymbol{x}$ is the original signal, λ denotes the regularization parameter, and $\Psi(\boldsymbol{x})$ represents the regularization term.

The iterative solution steps of TwISTA [12] for problem (1) can be written as

$$\begin{aligned} \boldsymbol{x}^{(1)} &= \Gamma_\lambda\left(\boldsymbol{x}^{(0)}\right) \\ \boldsymbol{x}^{(k+1)} &= (1-\gamma)\boldsymbol{x}^{(k-1)} + (\gamma-\eta)\boldsymbol{x}^{(k)} + \eta\Gamma_\lambda\left(\boldsymbol{x}^{(k)}\right) \end{aligned} \tag{2}$$

where $\boldsymbol{x}^{(0)}$ represents the initial value of $\boldsymbol{x}$ and γ and η are two parameters of the TwISTA method. $\Gamma_\lambda(\boldsymbol{x}^{(k)})(k > 0)$ is defined as

$$\begin{aligned} \Gamma_\lambda\left(\boldsymbol{x}^{(k)}\right) &= \mathrm{W}_\lambda\left(\boldsymbol{x}^{(k)} - \boldsymbol{\Phi}^{\mathrm{T}}\left(\boldsymbol{\Phi}\boldsymbol{x}^{(k)} - \boldsymbol{y}\right)\right) \\ \mathrm{W}_\lambda(\boldsymbol{h}) &= \arg\min_{z} \frac{1}{2}\|z - \boldsymbol{h}\|^2 + \lambda\Psi(z) \end{aligned} \tag{3}$$

where $\boldsymbol{\Phi}^{\mathrm{T}}$ is the transpose of $\boldsymbol{\Phi}$ and $\mathrm{W}_\lambda(\boldsymbol{h})$ denotes the proximal mapping with the input $\boldsymbol{h}$.

B. Proposed 2D-TwISTA

Based on the TwISTA, a 2D-TwISTA approach is developed for 2-D sparse ISAR imaging. First, the 2-D sparse ISAR signal model [2], [3], [4], [5], [6] can be expressed as

$$\mathbf{Y} = \mathbf{S}_r\mathbf{F}_r\mathbf{X}(\mathbf{S}_c\mathbf{F}_c)^{\mathrm{H}} + \mathbf{N} \tag{4}$$

where $\mathbf{Y} \in \mathbb{C}^{M\times N}$ is the 2-D sparse signal of 2-D CS measurements, $\mathbf{X} \in \mathbb{C}^{P\times Q}$ is the original ISAR image, $\mathbf{N}$ represents the additive complex Gaussian noise matrix, $\mathbf{S}_r\mathbf{F}_r \in \mathbb{C}^{M\times P}$ denotes the partial Fourier matrix in range dimension, and $\mathbf{S}_c\mathbf{F}_c \in \mathbb{C}^{N\times Q}$ represents the partial Fourier matrix in cross-range dimension.

To solve problem (4) efficiently utilizing the 2D-TwISTA method, (4) is first transformed into an optimization problem with l_1 norm, which can be represented as

$$\hat{\mathbf{X}} = \arg\min_{\mathbf{X}} \left\{ \frac{1}{2}\left\|\mathbf{S}_r\mathbf{F}_r\mathbf{X}(\mathbf{S}_c\mathbf{F}_c)^{\mathrm{H}} - \mathbf{Y}\right\|_F^2 + \lambda\|\mathbf{X}\|_1 \right\} \tag{5}$$

where $\|\cdot\|_F$ means the Frobenius norm. The iterative solution steps of 2D-TwISTA for problem (5) can be derived as

$$\begin{aligned} \mathbf{X}^{(1)} &= \Gamma_\lambda\left(\mathbf{X}^{(0)}\right) \\ \mathbf{X}^{(k+1)} &= (1-\gamma)\mathbf{X}^{(k-1)} + (\gamma-\eta)\mathbf{X}^{(k)} + \eta\Gamma_\lambda\left(\mathbf{X}^{(k)}\right) \end{aligned} \tag{6}$$

where γ and η are two parameters of the 2D-TwISTA. The initial value of $\mathbf{X}$ can be calculated as $\mathbf{X}^{(0)} = \mathbf{F}_r^{\mathrm{H}}\mathbf{S}_r^{\mathrm{H}}\mathbf{Y}\mathbf{F}_c\mathbf{S}_c$. $\Gamma_\lambda(\mathbf{X}^{(k)})(k > 0)$ can be derived as

$$\Gamma_\lambda\left(\mathbf{X}^{(k)}\right) = \mathrm{W}_\lambda\left(\mathbf{X}^{(k)} - \mathbf{F}_r^{\mathrm{H}}\mathbf{S}_r^{\mathrm{H}}\left(\mathbf{S}_r\mathbf{F}_r\mathbf{X}^{(k)}\mathbf{F}_c^{\mathrm{H}}\mathbf{S}_c^{\mathrm{H}} - \mathbf{Y}\right)\mathbf{S}_c\mathbf{F}_c\right) \tag{7}$$

where $\mathrm{W}_\lambda(\mathbf{H})$ represents the proximal mapping for the l_1 norm and can be expressed as

$$\mathrm{W}_\lambda(\mathbf{H}) = \arg\min_{\mathbf{Z}} \frac{1}{2}\|\mathbf{Z} - \mathbf{H}\|_F^2 + \lambda\|\mathbf{Z}\|_1. \tag{8}$$

The nonlinear problem (8) can be solved via the soft thresholding function [9] which can be represented as

$$\mathrm{W}_\lambda(\mathbf{H}) = \mathrm{sgn}(\mathbf{H})\max\{|\mathbf{H}| - \lambda, 0\} \tag{9}$$

where $\mathrm{sgn}(x) = 0$ when $|x| = 0$ and $\mathrm{sgn}(x) = x/|x|$ when $|x| > 0$. The Fourier matrices ($\mathbf{F_r}$ and $\mathbf{F_c}$) in the 2D-TwISTA are implemented utilizing FFT to improve the algorithm's efficiency.

C. Proposed L-2D-TwISTA

The main shortcoming of 2D-TwISTA is that it is sometimes challenging to select appropriate optimization parameters (e.g., γ and η) and requires multiple iterations to obtain satisfactory ISAR imaging results. The L-2D-TwISTA is proposed to solve this problem. First, the 2D-TwISTA method is iteratively unfolded into one stage of L-2D-TwISTA. Different from the 2D-TwISTA, the CV residual network is designed for solving the l_1 norm proximal mapping function in (8) instead of using the soft thresholding as the solution. By introducing the CV residual network, the training efficiency of the L-2D-TwISTA can be effectively enhanced, and more features of ISAR images can be acquired. The kth stage of the L-2D-TwISTA is shown in Fig. 1, which can be represented as

$$\begin{aligned} &\mathbf{X}^{(k+1)} \\ &= \left(1-\gamma^{(k)}\right)\mathbf{X}^{(k-1)} + \left(\gamma^{(k)} - \eta^{(k)}\right)\mathbf{X}^{(k)} \\ &\quad + \eta^{(k)}\mathbf{G}^{(k)} + \eta^{(k)}\mathrm{CConv}_4\mathrm{CConv}_1\left(\mathbf{G}^{(k)}\right) + \eta^{(k)} \\ &\quad \times \mathrm{CConv}_4\mathrm{CConv}_3\left(\mathrm{CReLu}\left(\mathrm{CConv}_2\left(\mathrm{CConv}_1\left(\mathbf{G}^{(k)}\right)\right)\right)\right) \end{aligned} \tag{10}$$

where $\mathbf{G}^{(k)} = \mathbf{X}^{(k)} - \mathbf{F}_r^{\mathrm{H}}\mathbf{S}_r^{\mathrm{H}}(\mathbf{S}_r\mathbf{F}_r\mathbf{X}^{(k)}\mathbf{F}_c^{\mathrm{H}}\mathbf{S}_c^{\mathrm{H}} - \mathbf{Y})\mathbf{S}_c\mathbf{F}_c$ and CReLu denotes the CV rectified linear unit (CV ReLu) in Fig. 1. CConv_1, CConv_2, CConv_3, and CConv_4 represent

Authorized licensed use limited to: SUN YAT-SEN UNIVERSITY. Downloaded on March 15,2025 at 02:07:22 UTC from IEEE Xplore. Restrictions apply.

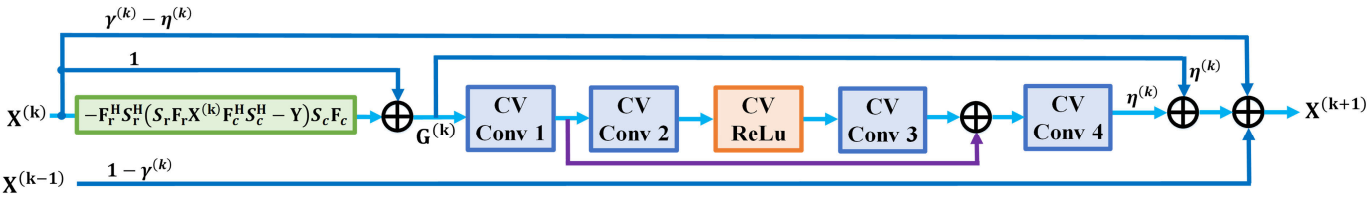

Fig. 1. kth stage of the proposed L-2D-TwISTA.

the four CV convolutional (CV Conv) layers from left to right in Fig. 1: CV Conv1, CV Conv2, CV Conv3, and CV Conv4. The number of input channels of CV Conv1 is 1, and the number of output channels is 32. The numbers of input and output channels for CV Conv2 and CV Conv3 are 32. The number of input channels of CV Conv4 is 32, and the number of output channels is 1. All the CV convolutions in L-2D-TwISTA adopt a 3×3 filter kernel size.

All parameters of the CV convolutions are different in each stage of L-2D-TwISTA. CV Conv2, CV ReLu, and CV Conv3 form the CV residual network. By introducing CV residual networks, L-2D-TwISTA's training stability can be enhanced. Moreover, the CV Conv layers and CV residual networks can not only realize the solution of the proximal mapping but also effectively improve the algorithm's ISAR image feature extraction ability. $\gamma^{(k)}$ and $\eta^{(k)}$ are the learnable parameters automatically updated during the training procedure. This process is carried out through backpropagation of L-2D-TwISTA, which can minimize the loss function by calculating the gradient to train the learnable parameter. The normalized root-mean-square error (NRMSE) is exploited as the loss function for L-2D-TwISTA, which can be expressed as

$$L(\boldsymbol{\theta}) = \frac{1}{|N_T|}\sum_{n=1}^{N_T}\frac{\left\|\hat{\mathbf{X}}_n(\mathbf{Y}_n,\boldsymbol{\theta})-\mathbf{X}_n\right\|_F}{\|\mathbf{X}_n\|_F} \tag{11}$$

where $\boldsymbol{\theta}$ denotes the trainable parameters of $\gamma^{(k)}$, $\eta^{(k)}$, CConv_1, CConv_2, CConv_3, CConv_4, and CReLu; N_T denotes the total number of training data; $\mathbf{Y}_n$ represents the nth 2-D sparse ISAR data of 2-D CS measurements; $\mathbf{X}_n$ is the nth trainable ISAR image; and $\hat{\mathbf{X}}_n$ is the reconstructed ISAR image utilizing the L-2D-TwISTA.

III. Experiments

A. Datasets

Due to the lack of measured ISAR datasets, simulated ISAR image and random scattering point image are used to build a 2-D sparse ISAR dataset. The center frequency of the transmit signal is 10 GHz; the bandwidth is 500 MHz, and the pulse repetition frequency is 100 Hz. The size of the simulated image is 256×256. The amplitude distribution of the simulated image is random to simulate the actual situation better. The positions of scattering points are randomly distributed, and the number of scattering points is randomly selected between 200 and 1000. A total of 600 simulated ISAR images are generated for model training. The signal-to-noise ratio is set as 10 dB. This part of the experiment only considers the ISAR image reconstruction process and assumes that motion compensation [5] and auto-focusing have been completed.

B. Experimental Details and Network Training

In the experiment, there are two methods that need to be trained using the previously constructed dataset: L-2D-ISTA and L-2D-TwISTA. Both L-2D-ISTA and L-2D-TwISTA are implemented in PyTorch, the CV residual network is used to solve the proximal mapping for l_1 norm, and the residual network structure is the same. The L-2D-ISTA and L-2D-TwISTA utilized the Adam optimizer for training with a learning rate of 0.0001. The initial parameter of step size for L-2D-ISTA is 0.1. The initial parameters for L-2D-TwISTA are $\gamma^{(0)} = 0.9$ and $\eta^{(0)} = 0.8$. Sparse sampling rates in the range and cross-range direction are 0.6 and 0.7, respectively. Therefore, the 2-D sparse sampling rates of the data are 0.36 and 0.49. The sampling positions of the sampling matrices are randomly generated, and the two sparse sampling rates correspond to the same number of sampling matrices. Sixty sampling matrices (including 30 2D-RMS matrices and 30 2D-GMS matrices) are constructed of each 2-D sparse sampling rate for the training of L-2D-ISTA and L-2D-TwISTA, and the number of training epochs is 200. The range–Doppler (RD) method, 2D-ISTA, and 2D-TwISTA are implemented in MATLAB R2022a. All experiments were conducted on the same computer with an Intel i5-12400F CPU and NVIDIA GeForce RTX 3060 GPU.

C. ISAR Image Evaluation Metrics

NRMSE, structural similarity (SSIM), and entropy (ENT) are selected as the evaluation indicators to quantitatively evaluate the 2-D sparse ISAR imaging results of different methods, which can be expressed as

$$\begin{aligned}
\mathrm{NRMSE} &= \frac{\left\|\hat{\mathbf{X}}-\mathbf{X}\right\|_F}{\|\mathbf{X}\|_F}\\
\mathrm{SSIM} &= \frac{(2\mu_{\hat{\mathbf{X}}}\mu_{\mathbf{X}}+D_1)(2\sigma_{\mathbf{X}\hat{\mathbf{X}}}+D_2)}{\left(\mu_{\hat{\mathbf{X}}}^2+\mu_{\mathbf{X}}^2+D_1\right)\left(\sigma_{\hat{\mathbf{X}}}^2+\sigma_{\mathbf{X}}^2+D_2\right)}\\
\mathrm{ENT} &= -\sum_{p=1}^{P}\sum_{q=1}^{Q}\frac{|\hat{\mathbf{X}}|^2}{E_{\hat{\mathbf{X}}}}\circ\ln\frac{|\hat{\mathbf{X}}|^2}{E_{\hat{\mathbf{X}}}}
\end{aligned} \tag{12}$$

where $\mathbf{X}$ represents the original ISAR image; $\hat{\mathbf{X}}$ denotes the ISAR imaging result of 2-D sparse data; and $\mu_{\hat{\mathbf{X}}}$ and $\mu_{\mathbf{X}}$ are the mean value of $|\hat{\mathbf{X}}|$ and $|\mathbf{X}|$, respectively. $\sigma_{\mathbf{X}}$ and $\sigma_{\hat{\mathbf{X}}}$ are the variances of $\hat{\mathbf{X}}$ and $\mathbf{X}$, respectively. $D_1 = (\nu_1 \max(|\hat{\mathbf{X}}|))^2$, $D_2 = (\nu_2 \max(|\mathbf{X}|))^2$, $\nu_1 = 0.01$, and $\nu_2 = 0.03$. $E_{\hat{\mathbf{X}}} = \sum_{p=1}^{P}\sum_{q=1}^{Q}|\hat{\mathbf{X}}|^2$ represents the total energy of the image $\hat{\mathbf{X}}$, and $\circ$ denotes the Hadamard product operation.

D. Comparison of Real ISAR Data Results

The measured Yak-42 aircraft data are utilized to verify the 2-D sparse ISAR imaging performance of the proposed

Authorized licensed use limited to: SUN YAT-SEN UNIVERSITY. Downloaded on March 15,2025 at 02:07:22 UTC from IEEE Xplore. Restrictions apply.

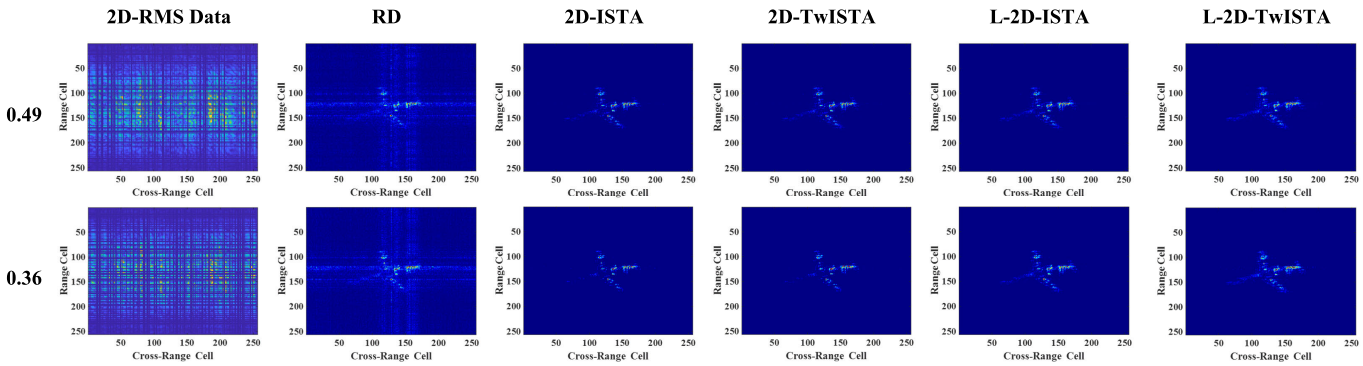

Fig. 2. Two-dimensional sparse ISAR imaging results of different methods under 2D-RMS real-measured data.

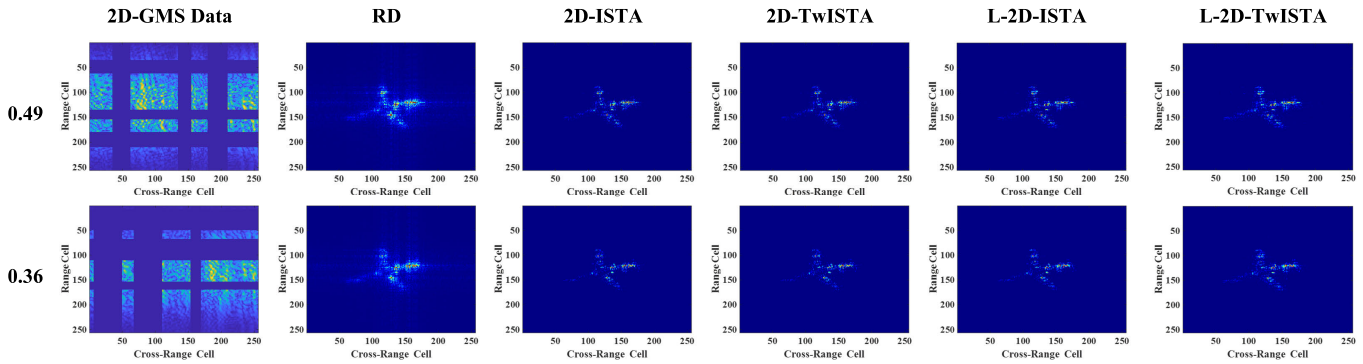

Fig. 3. Two-dimensional sparse ISAR imaging results of different methods under 2D-GMS real-measured data.

TABLE I
ISAR IMAGE QUALITY EVALUATION OF 2-D-RMS DATA UNDER DIFFERENT CS RATIOS

CS Ratio	Method	NRMSE	SSIM	ENT	Time(s)
0.49	RD	0.9878	0.5440	8.4073	**0.0009**
	2D-ISTA	0.2903	0.9170	**5.1313**	0.2991
	2D-TwISTA	0.2660	0.9206	5.2193	0.3195
	L-2D-ISTA	0.2509	0.9381	5.3027	0.0331
	L-2D-TwISTA	**0.1964**	**0.9568**	5.5134	0.0369
0.36	RD	1.2903	0.3783	9.0146	**0.0007**
	2D-ISTA	0.3575	0.9107	**5.0125**	0.2886
	2D-TwISTA	0.3211	0.9118	5.1219	0.3093
	L-2D-ISTA	0.2522	0.9361	5.3147	0.0252
	L-2D-TwISTA	**0.2095**	**0.9529**	5.5024	0.0276

TABLE II
ISAR IMAGE QUALITY EVALUATION OF 2D-GMS DATA UNDER DIFFERENT CS RATIOS

CS Ratio	Method	NRMSE	SSIM	ENT	Time(s)
0.49	RD	1.0158	0.7602	7.1936	**0.0009**
	2D-ISTA	0.5071	0.9035	**5.2902**	0.2934
	2D-TwISTA	0.5031	0.9060	5.2982	0.3145
	L-2D-ISTA	0.4786	0.9115	5.3139	0.0267
	L-2D-TwISTA	**0.4375**	**0.9286**	5.3574	0.0279
0.36	RD	1.1903	0.7625	7.2072	**0.0007**
	2D-ISTA	0.6921	0.8836	**5.1616**	0.2787
	2D-TwISTA	0.6797	0.8859	5.2110	0.3082
	L-2D-ISTA	0.6176	0.8893	5.2936	0.0245
	L-2D-TwISTA	**0.5536**	**0.9152**	5.4199	0.0259

L-2D-TwISTA method. The comparison methods include the RD algorithm, 2D-ISTA, 2D-TwISTA, and L-2D-ISTA. To be close to actual application scenarios, in this experiment, L-2D-TwISTA utilizes a single trained model to simultaneously handle 2-D sparse ISAR imaging problems with two different 2-D sparse sampling (2D-RMS and 2D-GMS) data and different sparse sampling rates. The results of different methods under 2D-RMS mode and 2D-GMS mode when the 2-D sparse sampling rates are 0.36 and 0.49 are shown in Figs. 2 and 3, respectively. Based on the previous image evaluation metrics, Tables I and II show the quantitative evaluation results of the 2-D sparse ISAR imaging results in Figs. 2 and 3, respectively. The smaller the NMRSE value, the higher the accuracy of 2-D sparse ISAR imaging, while the larger the SSIM value (-1 to 1), the more structural features of ISAR images are acquired. The minimum ENT does not necessarily mean the best result. With high image reconstruction accuracy, a larger ENT usually indicates that more ISAR image features have been obtained. As shown in Figs. 2 and 3 and Tables I and II, the RD algorithm will produce severe grating lobes and the worst imaging results compared to other methods due to directly performing the Fourier transform

Authorized licensed use limited to: SUN YAT-SEN UNIVERSITY. Downloaded on March 15,2025 at 02:07:22 UTC from IEEE Xplore. Restrictions apply.

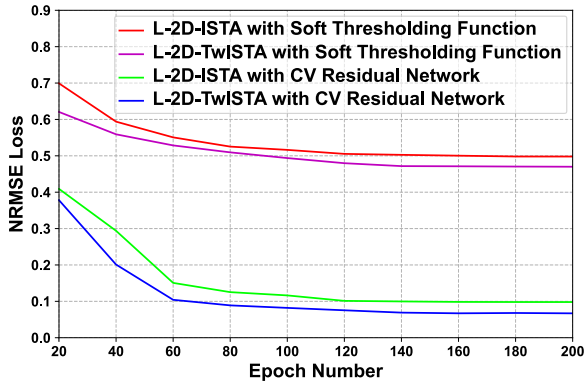

Fig. 4. Progression curves of NRMSE loss in the training phase for different approaches.

of 2-D sparse radar echoes. The 2D-ISTA and 2D-TwISTA algorithms can effectively remove grating lobes and preserve the main features of aircraft targets through multiple iterative solutions, achieving effective 2-D sparse ISAR imaging. The main disadvantage of 2D-TwISTA and 2D-ISTA compared to L-2D-TwISTA and L-2D-ISTA is that the optimization parameters need to be manually adjusted under different 2-D sparse ISAR imaging backgrounds (such as different imaging targets and different sparse sampling rates), which sometimes is not easy. Moreover, compared to 2-D-ISTA and 2D-TwISTA, the L-2D-ISTA and L-2D-TwISTA methods can preserve more ISAR image features by introducing CV convolutions and the CV residual network. The proposed L-2D-TwISTA has the best 2-D sparse ISAR imaging performance and can obtain the most ISAR image features compared to other methods. At the same time, the higher the 2-D sparse sampling rate, the better the 2-D ISAR imaging effect. Unlike the 2D-TwISTA method, the L-2D-TwISTA can learn appropriate optimization parameters from the ISAR data through a strong learning capacity. Compared with the 2D-TwISTA method, L-2D-TwISTA requires fewer iterations and has better 2-D sparse ISAR imaging performance. In this experiment, L-2D-TwISTA is only equivalent to six iterations of 2D-TwISTA to achieve satisfactory 2-D sparse ISAR imaging results.

E. Ablation Study

To further illustrate the benefits of introducing the CV residual network on network training, a comparative experiment is conducted between utilizing the soft thresholding function and CV residual network for solving the proximal mapping to implement the L-2D-TwISTA. In addition, the training process of the proposed L-2D-TwISTA is also compared with L-2D-ISTA. The progression curves of NRMSE loss in the training phase of different methods are shown in Fig. 4. By introducing the CV residual network, both L-2D-TwISTA and L-2D-ISTA achieve good training effects on the constructed 2-D sparse ISAR dataset. Since the amplitude distribution of ISAR images in the constructed dataset is random and there may be large differences between amplitude values, it is challenging to determine a suitable threshold to balance removing grating lobes or noise and retaining real image information. Therefore, using the soft thresholding function to implement L-2D-ISTA and L-2D-TwISTA will lead to poor training results. Consequently, introducing the CV residual network makes L-2D-TwISTA training more stable and enables the extraction of more ISAR image features.

IV. Conclusion

This letter proposes a novel L-2D-TwISTA method for high-efficiency and high-accuracy 2-D sparse ISAR imaging. By integrating the developed 2D-TwISTA and unfolding network strategy, the proposed L-2D-TwISTA can improve the network generalization capability and converge faster. Moreover, a CV residual network is designed in L-2D-TwISTA to solve the nonlinear problem of proximal mapping of the 2D-TwISTA, which can improve the network training efficiency and obtain more features of the ISAR images. The proposed L-2D-TwISTA can accomplish efficient 2-D sparse ISAR imaging and show good interpretability. The real-measured data results demonstrate that the L-2D-TwISTA can realize high-performance 2-D sparse ISAR imaging.

References

[1] J. Fan, S. Shao, and H. Liu, "High-Success-Rate and fast ISAR imaging of nonstationary moving platform-attitude rapidly changing ship target with DS evidence and minimum entropy theory," *IEEE Trans. Geosci. Remote Sens.*, vol. 62, 2024, Art. no. 5110215.

[2] H. R. Hashempour, "Sparsity-driven ISAR imaging based on two-dimensional ADMM," *IEEE Sensors J.*, vol. 20, no. 22, pp. 13349–13356, Nov. 2020.

[3] M. Lv, J. Yang, D. Wang, Y. Zhu, and W. Chen, "A structural sparse ISAR imaging method with joint phase autofocusing," *IEEE Geosci. Remote Sens. Lett.*, vol. 21, 2024, Art. no. 3509805.

[4] G. Xu, B. Zhang, J. Chen, and W. Hong, "Structured low-rank and sparse method for ISAR imaging with 2-D compressive sampling," *IEEE Trans. Geosci. Remote Sens.*, vol. 60, 2022, Art. no. 5239014.

[5] S. Shao, L. Zhang, and H. Liu, "High-resolution ISAR imaging and motion compensation with 2-D joint sparse reconstruction," *IEEE Trans. Geosci. Remote Sens.*, vol. 58, no. 10, pp. 6791–6811, Oct. 2020.

[6] Y. Wang, F. Dai, Q. Liu, Y. Liang, and X. Lu, "Fast SBL for 2-D joint super-resolution ISAR imaging with multidwell observation based on LC decomposition of fourth-order Toeplitz tensor," *IEEE Trans. Geosci. Remote Sens.*, vol. 62, 2024, Art. no. 5109517.

[7] Y. Wang, F. Dai, Q. Liu, and X. Lu, "2-D joint high-resolution ISAR imaging with random missing observations via cyclic displacement decomposition-based efficient SBL," *IEEE Trans. Geosci. Remote Sens.*, vol. 62, 2024, Art. no. 5111119.

[8] H. Li, J. Xu, H. Song, and Y. Wang, "Single-layer network realizes sparse aperture ISAR imaging," *IEEE Geosci. Remote Sens. Lett.*, vol. 21, pp. 1–5, 2024.

[9] H. Li, J. Xu, H. Song, and Y. Wang, "PIN: Sparse aperture ISAR imaging via self-supervised learning," *IEEE Geosci. Remote Sens. Lett.*, vol. 21, pp. 1–5, 2024.

[10] Z. Qing, S. Zhang, Y. Pu, and Z. Wen, "AF-DCDU-Net: An approach for ISAR autofocus imaging via deep convolution and deep unfolding net," *IEEE Geosci. Remote Sens. Lett.*, vol. 21, pp. 1–5, 2024, Art. no. 4016705.

[11] M. Lv, W. Chen, J. Yang, D. Wang, X. Wu, and X. Ma, "Joint 2-D sparse ISAR imaging and autofocusing by using 2-D-IADIANet," *IEEE Sensors J.*, vol. 23, no. 14, pp. 16428–16439, Jul. 2023.

[12] H. Gan, X. Wang, L. He, and J. Liu, "Learned two-step iterative shrinkage thresholding algorithm for deep compressive sensing," *IEEE Trans. Circuits Syst. Video Technol.*, vol. 34, no. 5, pp. 3943–3956, May 2024.

Authorized licensed use limited to: SUN YAT-SEN UNIVERSITY. Downloaded on March 15,2025 at 02:07:22 UTC from IEEE Xplore. Restrictions apply.